Solution for the statistical moments of scalar turbulence

Solution for the statistical moments of scalar turbulence

Matteo B. Bertagni*
Department of Land, Infrastructure and Environmental Engineering, Politecnico di Torino, Torino 10129, Italy

Massimo Marro and Pietro Salizzoni
Laboratoire de Mécanique des Fluides et d'Acoustique, University of Lyon, CNRS UMR 5509 Ecole Centrale de Lyon, INSA Lyon, Université Claude Bernard, 36, avenue Guy de Collongue, 69134 Ecully, France

Carlo Camporeale
Department of Land, Infrastructure and Environmental Engineering, Politecnico di Torino, Torino 10129, Italy

(Received 5 June 2019; published 20 December 2019)

We derive a system of equations for the statistical moments of a passive scalar dispersed in a turbulent flow from the transport equation of the probability density function. We solve the system through a Green's function and we obtain a formally exact solution for the statistical moments of the passive scalar concentration. We use this solution to achieve an analytical relationship for the second moment of a passive scalar released from a point source. Comparison with wind-tunnel experiments shows that the relationship is valid also in a neutral turbulent boundary layer if the reflection onto the ground and an appropriate model for the mixing timescale are considered. This approach, combined with a suitable model for the distribution of the concentration, allows the statistics of the passive scalar to be obtained in the whole domain in a closed and ready-to-use form.

DOI: 10.1103/PhysRevFluids.4.124701

I. INTRODUCTION

Turbulent flows transport and mix substances by moving parcels of fluids along chaotic trajectories. As a consequence, the substance concentration $C[\boldsymbol{x}, t]$ exhibits a complex turbulent dynamics, determined by the underlying velocity field, yet with its own decoupled statistics. This phenomenon, referred to as scalar turbulence [1–3], is ubiquitous in vast areas of physics, biology, and engineering and drives mixing and dispersion of key environmental and industrial processes. In atmospheric physics and environmental sciences [4], the research on scalar turbulence has been primarily devoted to determine the statistics of pollutant concentrations, due to both natural and anthropogenic releases (Fig. 1). The knowledge of these statistics is crucial, for example, to determine the risk for human health related to the exposure to an airborne toxic substance [5,6].

The main obstacle in achieving these statistics is given by the complexity of turbulence, which has so far prevented a theoretical solution for the one-point one-time probability density function (PDF) of the passive scalar concentration. In practical applications, suitable closed-form distributions are usually employed for rapid calculations. These distributions have been tested for decades with experimental and field data (e.g., Refs. [7–11]), and comprehend among others: the clipped-normal, the Lognormal, the Γ, the Weibull, the β, and, for the upper-tail of the PDF, the generalized Pareto distribution [12,13]. Although the debate on which distribution is the most representative perseveres, the Γ distribution probably deserves a special mention. Indeed, the Γ has been shown to nicely resemble the PDF for localized emissions in confined turbulence [14,15],

*matteo.bertagni@polito.it

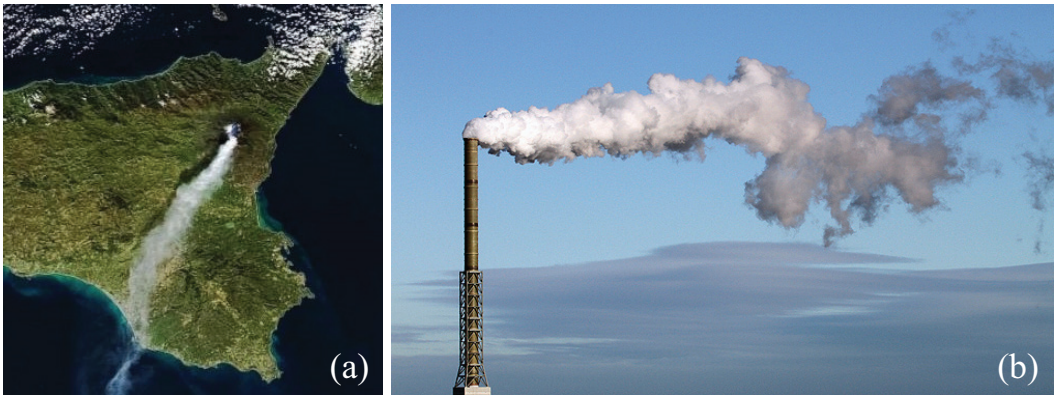

FIG. 1. Example of natural and anthropogenic scalar turbulence in the atmosphere. Smoke plumes from an eruption of the Etna Volcano in Italy (a) (Credit: Sentinel-3, Copernicus ESA), and an industrial chimney (b) (Credit: Walter Baxter https://www.geograph.org.uk/photo/3220320).

as well as in neutral boundary layers in field [16], and in flat-terrain [17,18] and urbanlike [19] wind tunnels.

A major advantage of the Γ, shared by the other two-parameter distributions, is that the full characterization of the concentration statistics only requires the knowledge of the mean $\langle C \rangle$ and the variance σ^2. The computation of $\langle C \rangle$ and σ^2 can be performed by means of a variety of numerical approaches (e.g., Refs. [20–23]). However, for operational purposes, it is worth disposing of analytical solutions for reference configurations, such as that of a localized release within the atmospheric boundary layer (see Fig. 1). A solution for $\langle C \rangle$ can be easily obtained adopting the so-called Gaussian models [24], which, in spite of the simplified hypotheses on which they rely, were showed to be successful in different contexts, ranging from atmosphere pollution [24] to fluvial, lacustrian, and oceanic dynamics [25]. Concerning the scalar variance σ^2, as far as we are aware, there is instead a gap in the current literature, only partially covered by empirical relationships (e.g., Ref. [26]) and the so-called meandering models (e.g., Refs. [18,27]). These latter models provide analytical solutions, but they require experiment-aided *ad hoc* calibrations and are thus of little practical use.

In this paper, under the framework of the so-called PDF methods (e.g., Refs. [28–32]), we present a formally exact solution for the statistical moments of C. The PDF methods are not novel in the subject, but they have been usually approached in a purely numerical way (e.g., Refs. [33–35]). In particular, we provide a closed relationship for the passive scalar variance σ^2, which, although it is obtained under the approximation of homogeneous and isotropic turbulence, will be shown to be valid also in the case of a plume emitted from a localized source within a turbulent boundary layer.

II. THE MATHEMATICAL MODEL

In statistically steady conditions, the transport equation for the one-point one-time PDF $p(\psi;\boldsymbol{x})$ of the concentration (whose relative sample space variable is here denoted as ψ) reads [30]

$$\boldsymbol{U}\nabla p = \nabla \cdot (\boldsymbol{K}\nabla p) + \tau_m^{-1}\partial_\psi[p(\psi - \langle C \rangle)], \tag{1}$$

where $\mathbf{U} = \langle \mathbf{u} \rangle$ is the mean velocity field, $\boldsymbol{K}[\boldsymbol{x}]$ is the turbulent diffusivity and τ_m the mixing timescale. To obtain Eq. (1), a gradient-diffusion model has been assumed for the convective flux $p\langle \mathbf{u}|\psi \rangle$ and an IEM model (interaction by exchange with the mean [20,30]) for the conditional Laplacian $\langle D\nabla^2 C|\psi \rangle$, where D is the molecular diffusivity.

Specifically, we here consider an x-oriented flow field with homogeneous mean velocity U inducing an advective mass flux that is significantly larger than its turbulent counterpart ($K_x \simeq 0$),

and whose statistics of velocity fluctuations are assumed to be homogeneous and isotropic (i.e., constant K_y, K_z, and τ_m, but see later).

The following convenient scaling is introduced:

$$X = \frac{x}{L}, \quad (Y, Z) = \sqrt{\frac{U}{K_{y,z} L}}\,(y, z), \quad \mathcal{A} = \frac{L}{\tau_m U}, \tag{2}$$

where L is a characteristic spatial scale. We multiply Eq. (1) for ψ^n and integrate, to eventually obtain a system of equations for the n-raw moments

$$\mathcal{L}_n \mu_n = n \mathcal{A} \mu_1 \mu_{n-1}, \tag{3}$$

where $\mathcal{L}_n = \partial_X - \partial_Y^2 - \partial_Z^2 + n\mathcal{A}$ (notice that $\mu_0 = 1$, $\mu_1 = \langle C \rangle$ and $\mu_2 = \langle C \rangle^2 + \sigma^2$).

For $n = 1$, Eq. (3) is a homogeneous linear partial differential equation, thereof solution reduces to the classical Gaussian model for the mean plume dispersion $\mu_1 = (m/X) \exp[-(Y^2 + Z^2)/4X]$, where m is a a constant to be determined through a boundary condition.

For $n > 1$, a solution to Eq. (3) is instead given in terms of the Green's function $G[\boldsymbol{X}, \boldsymbol{X}_0]$, such that

$$\mathcal{L}_n G[\boldsymbol{X}, \boldsymbol{X}_0] = \delta_D[\hat{\boldsymbol{X}}], \tag{4}$$

where $\delta_D[\cdot]$ is the δ function and the hat refers to the local reference frame centered in $\boldsymbol{X}_0$, i.e., $\hat{\mathbf{X}} = \mathbf{X} - \mathbf{X}_0$. After Fourier transforming, we get

$$G[\hat{\boldsymbol{X}}] = \frac{\theta[\hat{X}]}{4\pi \hat{X}} \exp\left[-n\mathcal{A}\hat{X} - \frac{\hat{Y}^2 + \hat{Z}^2}{4\hat{X}}\right], \tag{5}$$

where $\theta[\cdot]$ is the Heaviside function. Because of the property of the Dirac's function, we finally get an exact solution for the statistical moments ($n > 1$),

$$\mu_n = n\mathcal{A} \iiint_{-\infty}^{\infty} \mu_1[\boldsymbol{X_0}] \mu_{n-1}[\boldsymbol{X_0}] G[\hat{\boldsymbol{X}}] d\boldsymbol{X}_0. \tag{6}$$

We now consider the paradigmatic case of a localized source of diameter d_s placed at the origin of the reference frame at a height h_s from the ground and within a turbulent boundary layer of depth δ; see Fig. 2(a). In what follows, the latter is used as reference length scale, i.e., $\delta = L$. Since this configuration does not meet the requirements of homogeneous and isotropic turbulence, in the formulation of Gaussian models it is customary to adopt the following approximations: (i) U is taken as the velocity at the source height, (ii) K_z and K_y are taken constant when resolving the equations but space-dependent in the final formula. Notice that $2K_{y,z} = d\sigma_{y,z}^2/dt$, where σ_y and σ_z define the mean plume spread in the transversal and vertical directions, respectively, and can be determined, in absence of experimental measurements, through the classical approach by Taylor [36] (see Appendix A). In addition, the reflection onto the lower ground is solved through a mirror imaginary source, which introduces a wall correction to the classical Gaussian solution for the mean [24],

$$\mu_1 = \theta[X] \frac{m}{X} \left(\exp\left[-\frac{Y^2 + Z^2}{4X}\right] + \exp\left[-\frac{Y^2 + (Z + 2H_s)^2}{X}\right] \right), \tag{7}$$

where $m = \dot{M}/(4\pi\sqrt{K_y K_z} L)$ from mass conservation (where $\dot{M}$ is the passive scalar mass flux emitted at the source). With the above specifications, for $n = 2$ we obtain from Eq. (6)

$$\mu_2 = 2\mathcal{A} m^2 \int_{\xi}^{X} \left(\frac{\exp\left[-2\mathcal{A}(X - X_0) - \frac{Y^2 + Z^2}{2(2X - X_0)}\right]}{X_0(2X - X_0)} + r_2 \right) dX_0, \tag{8}$$

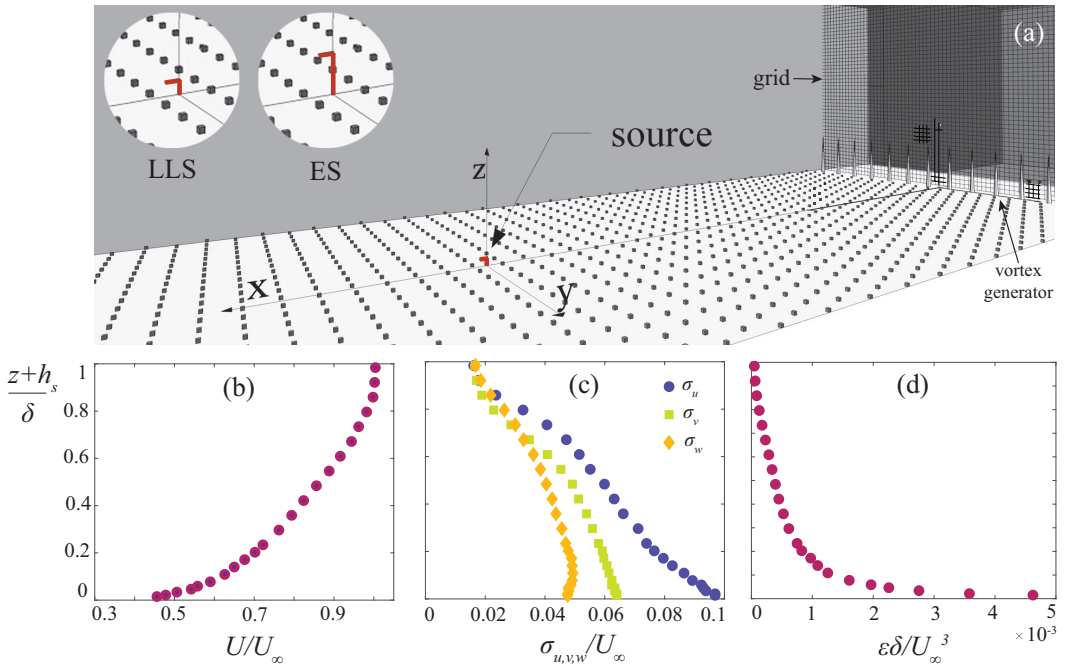

FIG. 2. (a) Sketch of the wind-tunnel setup showing the vortex generators and the turbulence grid at the entrance of the test section, the roughness elements on the floor, and the design of the lower level source (LLS) and the elevated source (ES) [38]. (b–d) Experimental velocity statistics within the turbulent boundary layer. Note that the z axis started at the ground in Nironi *et al.* [38], while here starts at the source height h_s.

where $\xi > 0$ is a parameter which depends on the source conditions, and r_2 is the reflection term

$$r_2 = \frac{1}{X_0(2X - X_0)} \exp\left[-2\mathcal{A}(X - X_0) - \frac{Y^2 + (2H_s + Z)^2}{2(2X - X_0)}\right] \times \left(1 + 2\exp\left[\frac{H_s(2H_sX_0 + X_0Z - H_sX)}{X_0(2X - X_0)}\right]\right), \tag{9}$$

where $H_s = h_s\sqrt{U/K_z L}$ is the dimensionless source height.

Equation (8) is our central result, namely the second moment of a passive scalar released from a point source in a turbulent flow. The longitudinal integral in Eq. (8) is analytically solvable only on the plume axis, if wall reflection is neglected, to yield

$$\mu_2 = m^2\mathcal{A}\left(\mathcal{B}_1\, e^{2AX} + \mathcal{B}_2\, e^{-2AX}\right)/X, \tag{10}$$

where $\mathcal{B}_1 = Ei[2\mathcal{A}\xi - 4\mathcal{A}X] - Ei[-2\mathcal{A}X]$, $\mathcal{B}_2 = Ei[2\mathcal{A}X] - Ei[2\mathcal{A}\xi]$ and $Ei[\cdot]$ refers to the exponential integral function [37].

III. EXPERIMENTAL SETUP

With the aim of testing the above theory, we have expanded the dataset of wind tunnel measurements previously published by two of the authors [38] with new data obtained in the same experimental setup. More specifically, Nironi *et al.* [38] performed wind-tunnel measurements of concentration up to a distance of $x/\delta = 5$ from the source. Here, the measurements have been extended to the very far-field, up to a distance of $x/\delta = 10$. The experiments were run in the atmospheric wind tunnel of the Laboratoire de Mécanique des Fluides et d'Acoustique at the Ecole

Centrale de Lyon, in France. This is a recirculating wind tunnel with a working section 14 m long and 3.7 m wide. To control the longitudinal pressure gradients the ceiling has a positive slope, so that the wind-tunnel height varies from 2 m at the entrance to 2.2 m at a distance of 7 m, and to 2.5 at its end. The wind-tunnel setup is sketched in Fig. 2(a). A neutrally stratified boundary layer of height $\delta = 0.8$ m was generated by combining the effect of a grid turbulence and a row of Irwin-type spires, placed at the beginning of the test section and spaced by a distance of 0.25 m, with roughness elements on the floor. The presence of a turbulence grid is not a usual feature of boundary-layer simulation systems and has been here used to minimize the inhomogeneities of the flow in the transverse direction. The entire working section floor was overlaid with cubes of 2-cm side acting as roughness elements, placed in a staggered array and covering approximately 1.8% of the tunnel floor surface. By imposing a free-stream velocity $U_\infty = 5$ m s^{-1}, the Reynolds number $Re = \delta U_\infty/\nu \sim 2.6 \times 10^5$ (ν is the kinematic viscosity of air) was sufficiently high to ensure the adequate simulation of a fully turbulent flow [39].

The velocity field was investigated by Nironi *et al.* [38] by means of a hot-wire constant temperature anemometer with an X-wire probe, which allowed two velocity components to be measured simultaneously. The instantaneous velocity is defined by the three components (u, v, w) in the (x, y, z) directions, respectively. The main velocity statistics needed for the present theory are presented as a function of the distance from the ground in Figs. 2(b)–2(d), where the vertical profiles of mean longitudinal velocity $U = \langle u \rangle$, the root mean square of the three velocity components $\sigma_{u,v,w}$ and the turbulent kinetic energy dissipation rate ε are reported. This latter was estimated as $\varepsilon = 15\nu\langle \partial_t u' \rangle^2/U^2$, i.e., adopting the Taylor frozen-turbulence hypothesis and assuming local isotropy of the velocity field.

Ethane (C_2H_6) was used as a tracer in the experiments, since it has a density similar to air, and was continuously discharged from a source of varying diameter and elevation. The sources consisted of a metallic L-shaped tube and were placed where the boundary layer can be considered fully developed. As in Ref. [38], the following acronyms are used for the source configurations: ES3 for the Elevated Source ($h_s = 152$ mm) with small diameter ($d_s = 3$ mm), ES6 for the Elevated Source ($h_s = 152$ mm) with big diameter ($d_s = 6$ mm), and LLS3 for the Lower Level Source ($h_s = 48$ mm) with small diameter ($d_s = 3$ mm). The results for LLS6 ($h_s = 40$ mm and $d_s = 6$ mm) come from new measurements performed on the plume axis.

Concentration measurements were made with a fast flame ionization detector (FID) [40] with a sampling tube 0.3 m long, which allowed us to acquire concentration signals with a frequency of 800 Hz. The sampling frequency is sufficiently high to correctly capture the intermittency of the concentration signal in the near field [41]. The time series of concentration were measured for 300 s. To take into account of the drift induced by the recirculation of air in the wind tunnel, the background concentrations were recorded before and after acquiring any of the concentration time series. The background concentration, which was assumed to evolve linearly with time from its initial to its final value, was then subtracted from the signals.

IV. MODEL VALIDATION

The reliability of the theoretical model is now tested against the wind-tunnel dataset of Nironi *et al.* [38], which has been here extended with new measurements. Moreover, data from Fackrell and Robins [42] are also used. These datasets contain concentration statistics downwind a localized source of varying diameter and elevation within a turbulent boundary layer.

A. Source parameter and mixing timescale

To validate the theory we are required to set: (i) the lower integration bound ξ in Eq. (8) and (ii) the mixing timescale τ_m.

The former parameter, ξ, is a small positive value, that we introduce to avoid the singularity in the integral Eq. (8) at $X_0 = 0$. This parameter must be linked to the source conditions. Indeed,

experiments have shown that the ratio between the initial size of the plume (scaling with the source diameter d_s) and the largest eddy (scaling with the source height h_s) highly affects the statistics of the concentration fluctuations near the source [38,43]. Best fitting with the experiments suggests $\xi = (d_s/h_s)^{10}$. As ξ is numerically small, a methodology to solve the integral in Eq. (8) is required (this is presented in the Appendix B).

Concerning the mixing timescale τ_m, the IEM model is known to be exact only in the ideal case of an initially Gaussian scalar PDF in homogeneous turbulence [30]. Yet, the IEM model is also used for its simplicity in numerical simulations of not-ideal cases by assuming a constant of proportionality between τ_m and the turbulent timescale $\tau = k/\varepsilon$, where k is the turbulent kinetic energy and ε its rate of dissipation (e.g., Ref. [2]). More complicated formulations, which account for the spatial variability of τ_m, are also available. In such formulations, the classical assumption [44] is that the total plume dispersion is the consequence of two physical processes: the fluctuations of the plume centroid (meandering motion) and the relative dispersion around the plume centroid, but only the latter process is considered to influence the mixing timescale. A notable example of these formulations is the closed model by Cassiani *et al.* [45], who defined the mixing timescale as

$$\tau_m^{(x)} = \alpha \frac{\sigma_r}{\sigma_{\boldsymbol{u}r}}, \tag{11}$$

where α is an empirical constant, σ_r is the relative plume spread around the plume's centroid, and the superscript (x) highlights the x-dependence of τ_m in this formulation. $\sigma_{\boldsymbol{u}r}$ is the root-mean square of the fluctuations of relative velocity, i.e., the difference between the turbulent velocity and the instantaneous velocity of the plume centroid. This latter quantity is usually modeled as [23,45]

$$\sigma_{\boldsymbol{u}r}^2 = \sigma_{\boldsymbol{u}}^2 \left(\frac{\sigma_r}{L_E} \right)^{2/3}, \tag{12}$$

where $L_E = (3\sigma_{\boldsymbol{u}}/2)^{3/2}\varepsilon$ is the Eulerian integral scale, and $\sigma_{\boldsymbol{u}}^2$ is evaluated, because of the inhomogeneity of the turbulent field, as the average of the variances of the three velocity components. When the plume size reaches the Eulerian integral scale, i.e., $\sigma_r = L_E$, meandering becomes negligible with respect to relative dispersion in the plume spread, so that $\sigma_{\boldsymbol{u}r} = \sigma_{\boldsymbol{u}}$. The relative plume spread can be evaluated as

$$\sigma_r^2 = \frac{C_r\varepsilon(t_0 + t_f)^3}{1 + \left[C_r\varepsilon(t_0 + t_f)^3 - d_s^2\right]/\left(d_s^2 + 2\sigma_{\boldsymbol{u}} T_L t_f\right)}, \tag{13}$$

where $t_0 = (d_s^2/C_r\varepsilon)^{1/3}$ is the inertial formulation for a dispersion from a finite source size [8], $t_f = x/U$ is the flight time, and $T_L = 2\sigma_{\boldsymbol{u}}^2/C_0\varepsilon$ is the Lagrangian timescale. The Richardson and Kolmogorov constants read $C_r = 0.3$ and $C_0 = 4.5$, respectively [23], while the constant $\alpha = 0.65$ for Eq. (11) is obtained from a best fit with experiments.

In this Paper, we use two formulations for τ_m: a constant value, $\tau_m^{(c)} = 0.44\tau$, and the x-dependent $\tau_m^{(x)}$ from Eq. (11) [see the solid and dash-dot lines in Fig. 3(a)]. Regarding the latter formulation, we stress out that $\tau_m^{(x)}$ is considered x-dependent just in the final formula, as done for the turbulent diffusivities K_y and K_z.

B. Comparison with experiments

In Figs. 3(b) and 3(c), we report the intensity of the concentration fluctuations, $\sigma/\langle C\rangle$, along the plume axis for different experimental setups and source diameters. In agreement with the experiments, the statistical moments in the far field are independent of the source diameter. The results with the formulation $\tau_m^{(c)}$ (solid lines) show that the concentration fluctuations are correctly provided in the proximity to the source, where the dispersion process is mainly governed by the meandering motion of the small-scale plume ($\sigma/\langle C\rangle > 1$), and systematically underestimated in the far field, where relative dispersion becomes the key physical process in the plume spread ($\sigma/\langle C\rangle < 1$). The opposite is obtained when $\tau_m^{(x)}$ from Eq. (11) is used (dash-dot lines). Indeed,

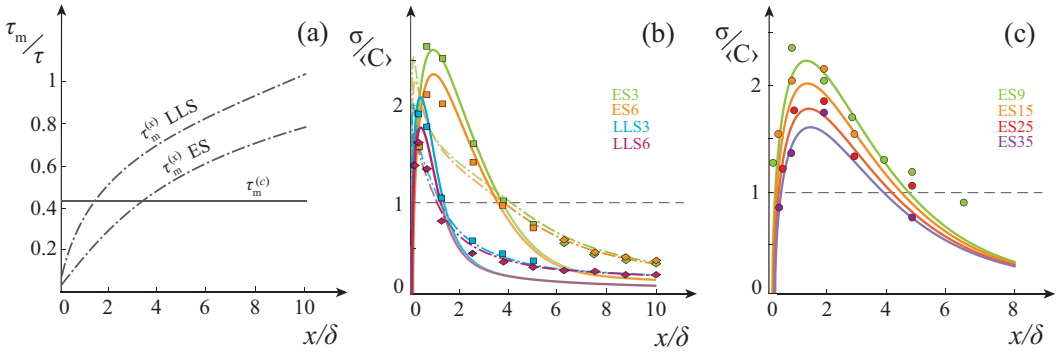

FIG. 3. Mixing timescale (a) and intensity of the concentration fluctuations (b, c) along the plume axis for different source conditions. Solid ($\tau_m^{(c)}$) and dash-dot ($\tau_m^{(x)}$) lines refer to the present theory. Symbols are the experimental data of Nironi *et al.* [38] (squares), the new experiments (diamonds) and Fackrell and Robins [42] (circles). Numbers in LLS and ES acronyms refer to the source diameter in mm.

this latter model more solidly considers the effect of relative dispersion in the evaluation of τ_m. Overall, through an appropriate matching between the two formulations of τ_m ($\tau_m^{(c)}$ for the meandering-dominated regime and $\tau_m^{(x)}$ for the relative dispersion-dominated one), it is possible to correctly define the concentration fluctuations throughout the domain. From a practical point of view, thi means that both models of the mixing timescale have to be used for the evaluation of the concentration fluctuations, and the results have to be matched at $\sigma/\langle C\rangle \sim 1$.

This appears clear also in Fig. 4, where some vertical and transverse distributions of $\langle C\rangle$ and σ are reported (additional plots are provided in Figs. 6–10). In the proximity of the source, both $\langle C\rangle$ and σ exhibit Gaussian distributions. Further from the source, the vertical profiles are influenced by the presence of the lower boundary, while the lateral distributions preserve the axial symmetry. The

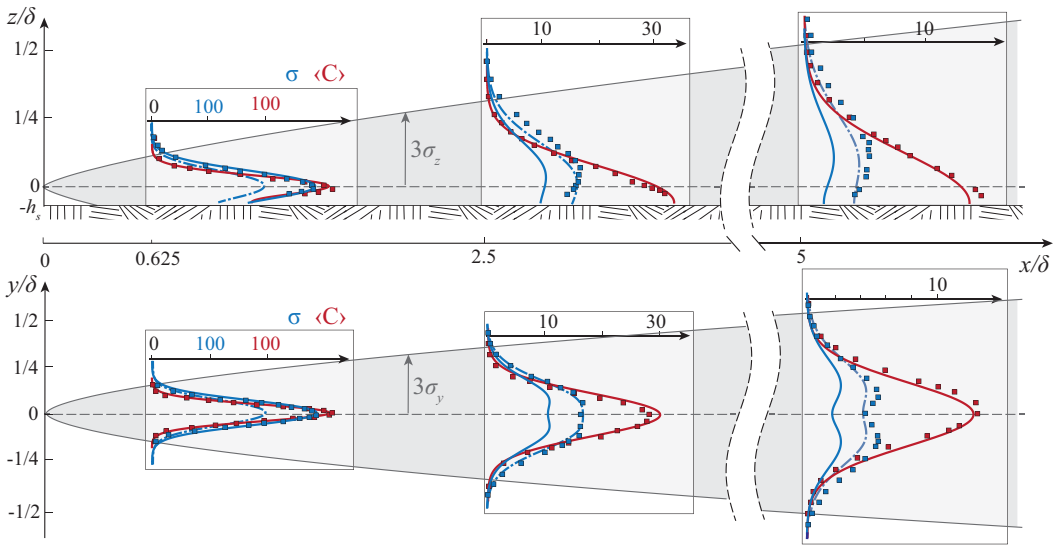

FIG. 4. Vertical and transverse profiles of mean (red) and standard deviation (blue) of the concentration at increasing distance downstream of the source. Solid ($\tau_m^{(c)}$) and dash-dot ($\tau_m^{(x)}$) lines refer to the theory, while symbols correspond to experimental data LLS3 [38]. For continuity with Nironi *et al.* [38], lengths and concentration are scaled with δ and $\dot{M}U_\infty^{-1}\delta^{-2}$, respectively (where U_∞ the free-stream velocity).

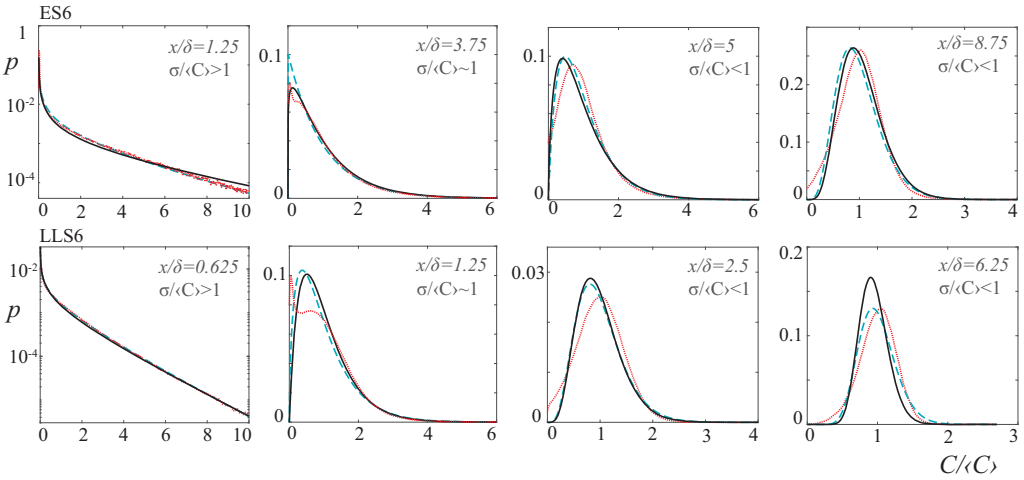

FIG. 5. One-point one-time PDFs on the plume axis at different distances from the source. Red dotted lines are the experimental PDFs. Dashed blue lines are the Γ distributions –Eq. (14), with experimental mean and variance. Solid black lines are the Γ distributions with mean and variance from Eqs. (7) and (8).

Gaussian model Eq. (7) and the analytical solution Eq. (8) very well reproduce the experimental values for $\langle C \rangle$ and σ. Notably, in the far-field transverse profile (right-low panel), Eq. (8) correctly identifies the decrease of σ in the plume core and the appearance of the two side peaks. This change in the qualitative behavior of σ is caused by the increasing size of the plume spread that, far from the source, overcomes the size of the turbulent eddies. Therefore, while in the near field the turbulent eddies entrain fresh air, which enhances the concentration fluctuations, in the far field the eddies just promote a local mixing within the plume core, leading to lower concentration fluctuations.

The knowledge of $\langle C \rangle$ and σ, combined with a proper model for the one-point PDF, allows the passive scalar statistics to be fully defined throughout the domain. For the experimental dataset of Nironi *et al.* [38], the best distribution was shown to be the Γ,

$$p_\Gamma = \frac{\lambda^\lambda C^{\lambda-1}}{\Gamma[\lambda]\langle C \rangle^\lambda} e^{-\lambda C/\langle C \rangle}, \tag{14}$$

where $\lambda = \langle C \rangle^2/\sigma^2$ and $\Gamma[\cdot]$ is the Γ special function [37]. Accordingly, in Fig. 5 we compare the experimental PDFs to the Γ distributions obtained with experimental and theoretical values for $\langle C \rangle$ and σ. Indeed, the Γ distributions are shown to nicely resemble the experimental PDFs in the whole domain, ranging from the meandering-dominated regime, where the large-scale fluctuations cause the PDF to be exponential-like (first column), to the far field, where the effect of the meandering motion becomes negligible and relative dispersion leads to Gaussian-like distributions (third and fourth columns). The second column of Fig. 5 highlights the transition from the meandering-dominated regime to relative dispersion one ($\sigma/\langle C \rangle \sim 1$).

We stress out that a broader graphical comparison between theoretical estimates and experimental data for $\langle C \rangle$ and σ is provided in Figs. 6–10.

V. DISCUSSION AND CONCLUSIONS

To sum up, we obtained a formally exact solution for the statistical moments of a passive scalar dispersed in a turbulent flow, Eq. (6). This result was used to derive a new closed relationship for the second moment of concentration in the case of an emission from a point source, Eq. (8). The analytical relationship Eq. (8) very well fits the experiments throughout the domain (Figs. 3 and 4), besides very close to the source ($x \to 0$), if two formulations for the mixing timescale are

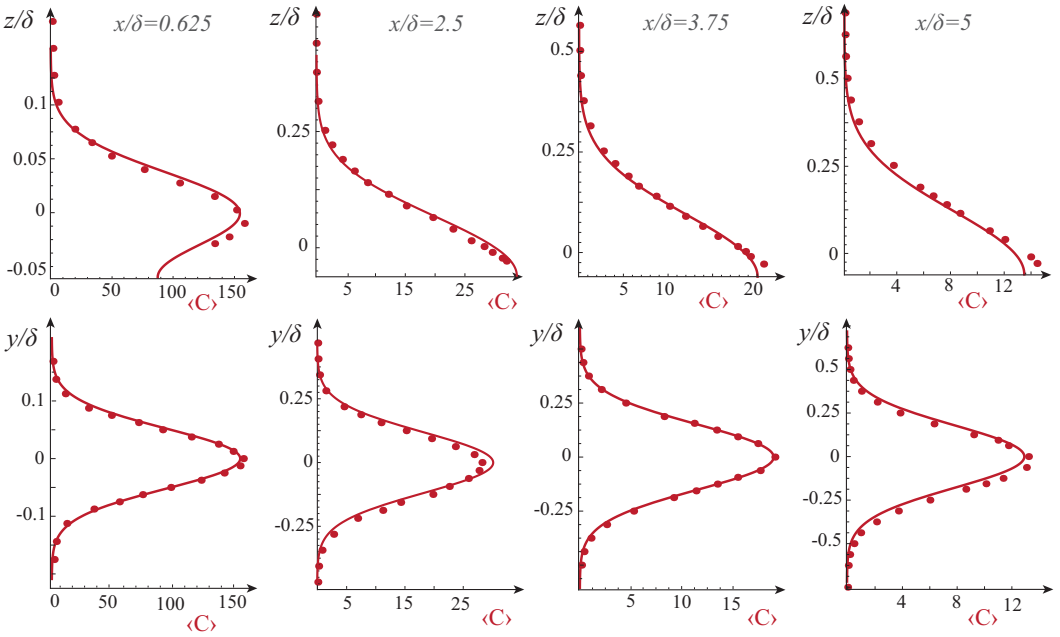

FIG. 6. Mean plume spread for the LLS3. The points are the experimental values, the solid lines are the Gaussian model Eq. (7). To account for the inhomogeneity of the velocity field close to the lower boundary, the velocity U is estimated at the height of the plume center of mass [38].

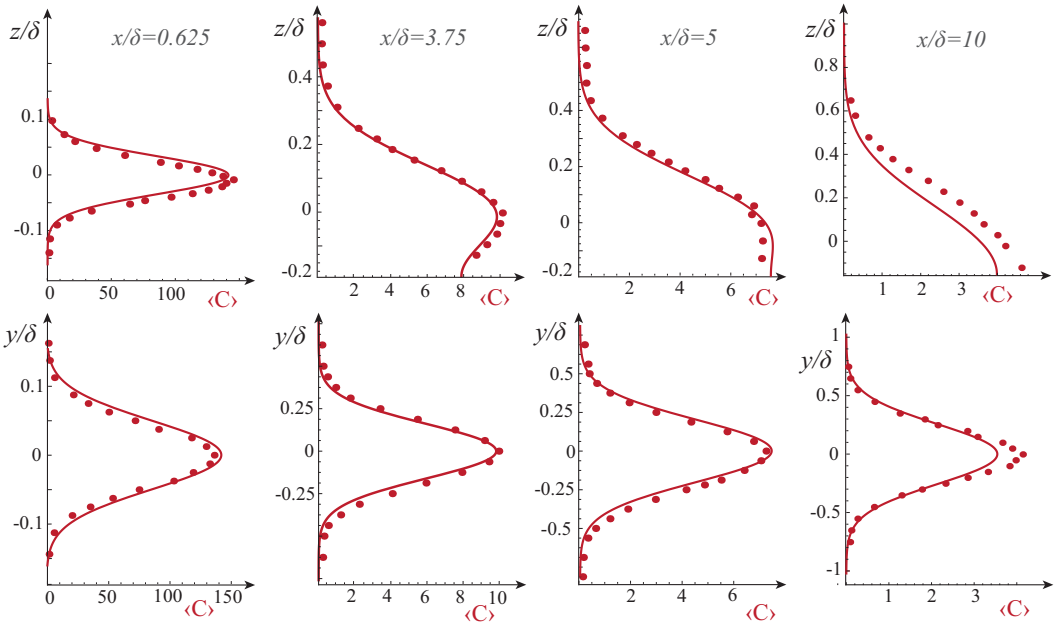

FIG. 7. Mean plume spread for the elevated sources ES6. Notice that, as the mean is affected by the source diameter just in proximity of the source, there is no need to discriminate between ES3 and ES6 [38].

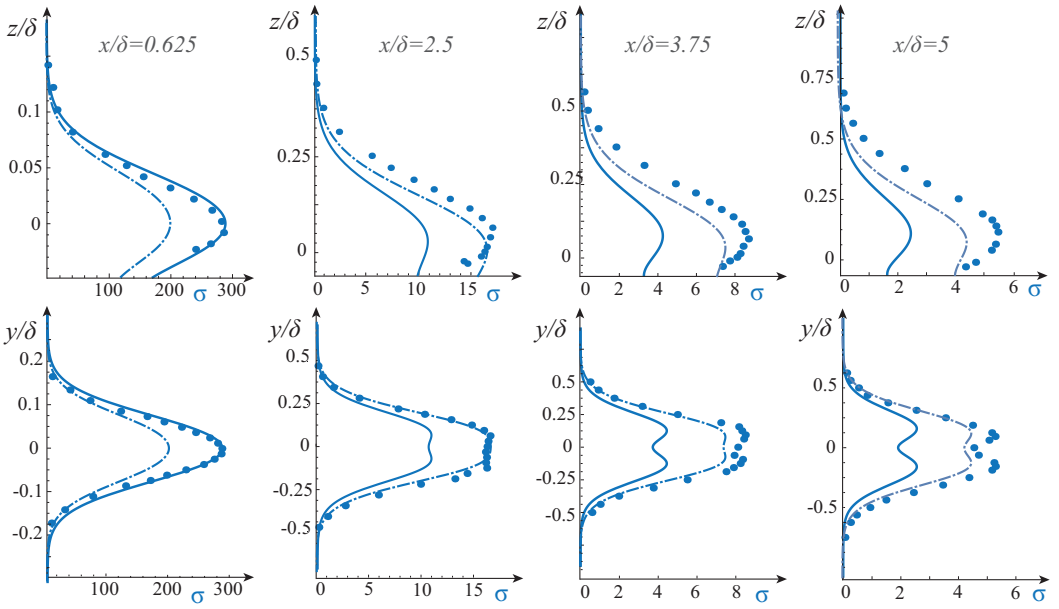

FIG. 8. Standard deviation for the LLS3. The points are the experimental values; the solid and dash-dot lines come from Eq. (8), with $\tau_m^{(c)}$ and $\tau_m^{(x)}$, respectively.

considered: $\tau_m^{(c)}$ in the meandering-dominated regime ($\sigma/\langle C\rangle < 1$) and $\tau_m^{(x)}$ in the relative-dispersion regime ($\sigma/\langle C\rangle > 1$). The necessity of this discrimination is due to the well-known shortcomings of the IEM model, which was already shown to undervalue the concentration fluctuations by introducing spurious fluxes [20,21]. Yet, the simplicity of the IEM model allows us to obtain an

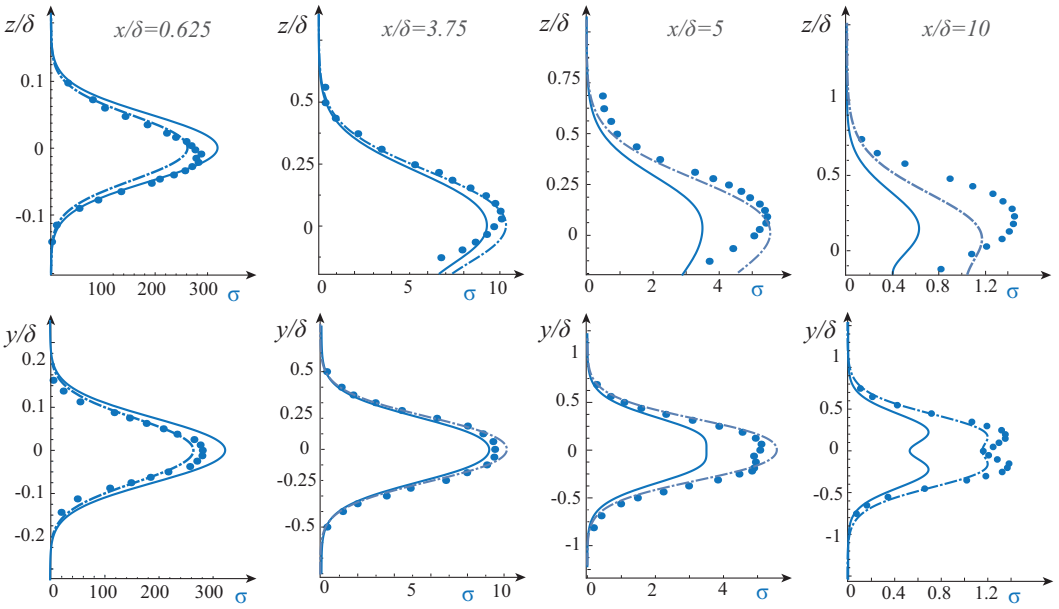

FIG. 9. Standard deviation for the elevated source ES6.

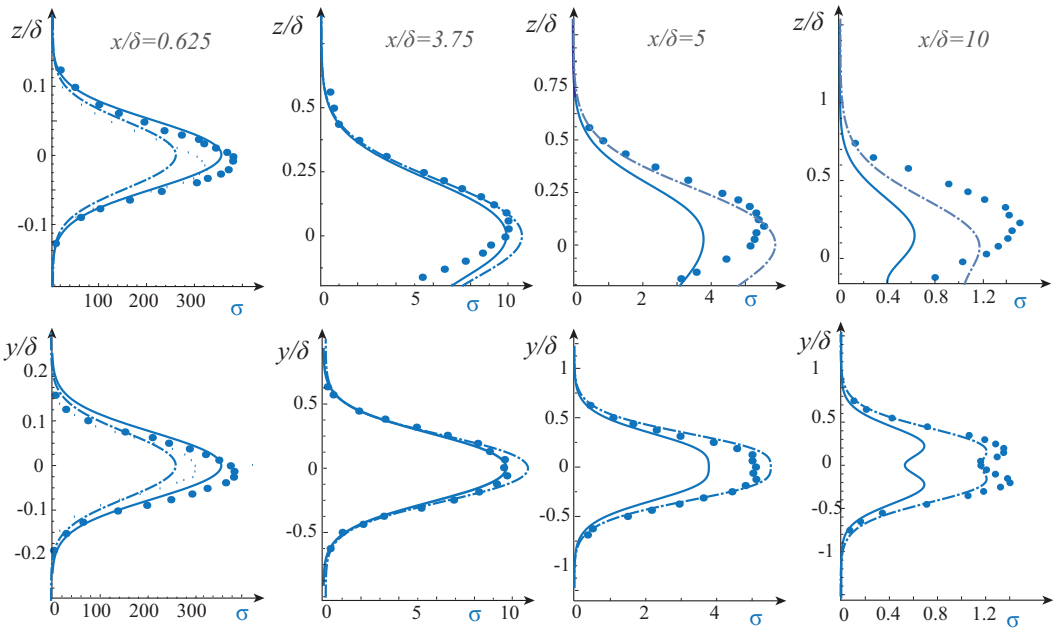

FIG. 10. Standard deviation for the elevated source ES3.

analytical solution for the passive scalar variance, while more sophisticated closures for the effect of molecular diffusivity [23,46,47] would probably require a numerical approach.

The integral in Eq. (8) currently limits the possibility to obtain closed relationships for higher order statistical moments. However, by assuming an appropriate model for the PDF, as the Γ distribution Eq. (14) [38], the full statistics of the passive scalar can be defined in the whole domain in a fast and simple way (Fig. 5). Nonetheless, the PDF gives no information on the temporal dynamics of the concentration, which is fundamental to determine for instance the exposure times to a toxic substance. Stochastic models (e.g., Refs. [48,49]) are a useful tool for this purpose. However, these models are currently little used, as they require the definition of a proper timescale and the intensity of the concentration fluctuations, which are usually obtained from empirical relations or experiments. In this perspective, the novel relation Eq. (8) provides an easy way to define the latter parameter and thus increase the applicability of such stochastic models. To conclude, the present theory can serve atmospheric scientists and environmental engineers for operational purposes, for example, to rapidly predict the statistics of atmospheric pollutant concentrations in statistically steady flow conditions and domains without orographical complexity.

ACKNOWLEDGMENTS

P.S. acknowledges the Région Auvergne Rhône Alpes Project SCUSI. This work was partially supported by Società Metropolitana Acque Torino (SMAT).

APPENDIX A: TURBULENT DIFFUSIVITY K

In the framework of Gaussian models for plume dispersion, the transverse and vertical turbulent diffusivities are defined as $(K_y, K_z) = (\sigma_y^2, \sigma_z^2)/2t_f$, where $t_f = x/U$ is the flight time. In the

absence of experimental measurements, the mean plume dispersion may be formulated through the classical Taylor's relationships [36],

$$\sigma_y^2 = \frac{d_s^2}{6} + 2\sigma_v^2 T_{L,v}\left\{t_f - T_{L,v}\left[1 - \exp\left(-\frac{t_f}{T_{L,v}}\right)\right]\right\}, \tag{A1}$$

$$\sigma_z^2 = \frac{d_s^2}{6} + 2\sigma_w^2 T_{L,w}\left\{t_f - T_{L,w}\left[1 - \exp\left(-\frac{t_f}{T_{L,w}}\right)\right]\right\}, \tag{A2}$$

where $T_{L,v} = 2\,\sigma_v^2/(\varepsilon\, C_0)$ and $T_{L,w} = 2\,\sigma_w^2/(\varepsilon\, C_0)$ are the Lagrangian vertical and transverse timescales, and $C_0 = 4.5$ is the Kolmogorov constant [38]. In this paper, we use the experimental values for $\sigma_{y,z}$, as Nironi *et al.* [38] had noticed that they slightly differ from Taylors predictions Eqs. (A1) and (A2).

APPENDIX B: HINTS TO SOLVE THE INTEGRAL FOR μ_2

We here suggest how to deal with the integral (8), whose lower bound ξ is numerically small (ranging from 10^{-10} for the LLS to 10^{-18} for the ES). First, the integral Eq. (8) is split in the longitudinal domain, so that

$$\mu_2 = 2\mathcal{A}\,m^2 \int_\xi^X g(\mathbf{X}, X_0)\, dX_0 = 2\mathcal{A}\,m^2\left[\int_\xi^\varphi g(\mathbf{X}, X_0) dX_0 + \int_\varphi^X g(\mathbf{X}, X_0) dX_0\right], \tag{B1}$$

where $\varphi \ll 1$ is a small value, but big enough to not provide numerical issues when solving the second integral in the right-hand side of Eq. (B1). The integral between ξ and φ regards the very proximity to the source. Thus, the reflection term can be neglected and as $X_0 \ll 1$, the integrand function g can be expanded in a first order series of X_0. By doing so, the integral can be analytically solved to eventually provide

$$\int_\xi^\varphi g(\mathbf{X}, X_0) dX_0 \sim \left[\frac{\log(\varphi/\xi)}{2X} + F\right] \exp\left(-2\mathcal{A}X - \frac{Y^2 + Z^2}{4X}\right), \tag{B2}$$

where F is a function with small numerical influence, which reads

$$F = -\frac{1}{512X^5}(\xi - \varphi)[256\mathcal{A}X^4(\Delta + 1) + 128X^3\Delta - 32X^2(R^2\Delta - \phi) - 16X\phi R^2 + \phi R^4], \tag{B3}$$

where $R^2 = Y^2 + Z^2$, $\phi = \xi + \varphi$, and $\Delta = (\mathcal{A}\phi + 1)$.

[1] B. Shraiman and E. Siggia, Scalar turbulence, Nature **405**, 639 (2000).
[2] Z. Warhaft, Passive scalars in turbulent flows, Annu. Rev. Fluid Mech. **32**, 203 (2000).
[3] E. Villermaux, Mixing versus stirring, Annu. Rev. Fluid Mech. **51**, 245 (2019).
[4] J. Hunt, Turbulent diffusion from sources in complex flows, Annu. Rev. Fluid Mech. **17**, 447 (1985).
[5] M. Kampa and E. Castanas, Human health effects of air pollution, Environ. Pollut. **151**, 362 (2008).
[6] A. Gunatilaka, A. Skvortsov, and R. Gailis, A review of toxicity models for realistic atmospheric applications, Atmos. Environ. **84**, 230 (2014).
[7] W. Lewellen and R. Sykes, Analysis of concentration fluctuations from lidar observations of atmospheric plumes, J. Clim. Appl. Meteorol. **25**, 1145 (1986).
[8] P. Franzese, Lagrangian stochastic modeling of a fluctuating plume in the convective boundary layer, Atmos. Environ. **37**, 1691 (2003).
[9] J. Bartzis, G. Efthimiou, and S. Andronopoulos, Modeling short-term individual exposure from airborne hazardous releases in urban environments, J. Hazard. Mater. **300**, 182 (2015).

[10] E. Yee, P. Kosteniuk, G. Chandler, C. Biltoft, and J. Bowers, Recurrence statistics of concentration fluctuations in plumes within a near-neutral atmospheric surface layer, Bound.-Lay. Meterol. **66**, 127 (1993).
[11] D. J. Wilson, *Concentration Fluctuations and Averaging Time in Vapor Clouds* (John Wiley & Sons, New York, 2010).
[12] R. Munro, P. Chatwin, and N. Mole, The high concentration tails of the probability density function of a dispersing scalar in the atmosphere, Bound.-Lay. Meterol. **98**, 315 (2001).
[13] N. Mole, T. P. Schopflocher, and P. J. Sullivan, High concentrations of a passive scalar in turbulent dispersion, J. Fluid Mech. **604**, 447 (2008).
[14] E. Villermaux and J. Duplat, Mixing as an Aggregation Process, Phys. Rev. Lett. **91**, 184501 (2003).
[15] J. Duplat and E. Villermaux, Mixing by random stirring in confined mixtures, J. Fluid Mech. **617**, 51 (2008).
[16] E. Yee, P. Kosteniuk, G. Chandler, C. Biltoft, and J. Bowers, Statistical characteristics of concentration fluctuations in dispersing plumes in the atmospheric surface layer, Bound.-Lay. Meterol. **65**, 69 (1993).
[17] E. Yee and A. Skvortsov, Scalar fluctuations from a point source in a turbulent boundary layer, Phys. Rev. E **84**, 036306 (2011).
[18] M. Marro, C. Nironi, P. Salizzoni, and L. Soulhac, Dispersion of a passive scalar fluctuating plume in a turbulent boundary layer. Part II: Analytical modeling, Bound.-Lay. Meterol. **156**, 447 (2015).
[19] G. Efthimiou, S. Andronopoulos, I. Tolias, and A. Venetsanos, Prediction of the upper tail of concentration distributions of a continuous point source release in urban environments, Environ. Fluid Mech. **16**, 899 (2016).
[20] B. Sawford, Micro-mixing modeling of scalar fluctuations for plumes in homogeneous turbulence, Flow, Turbul. Combust. **72**, 133 (2004).
[21] M. Cassiani, A. Radicchi, J. Albertson, and U. Giostra, An efficient algorithm for scalar PDF modeling in incompressible turbulent flow: Numerical analysis with evaluation of IEM and IECM micro-mixing models, J. Comput. Phys. **223**, 519 (2007).
[22] J. Lin, D. Brunner, C. Gerbig, A. Stohl, A. Luhar, and P. Webley, *Lagrangian modeling of the atmosphere*, Vol. 200 (John Wiley & Sons, New York, 2013).
[23] M. Marro, P. Salizzoni, L. Soulhac, and M. Cassiani, Dispersion of a passive scalar fluctuating plume in a turbulent boundary layer. Part III: Stochastic modeling, Bound.-Lay. Meterol. **167**, 349 (2018).
[24] S. Arya, *Air Pollution Meteorology and Dispersion*, Vol. 6 (Oxford University Press, New York, 1999).
[25] H. B. Fischer, J. E. List, C. R. Koh, J. Imberger, and N. H. Brooks, *Mixing in Inland and Coastal Waters* (Elsevier, Amsterdam, 2013).
[26] P. Chatwin and P. J. Sullivan, A simple and unifying physical interpretation of scalar fluctuation measurements from many turbulent shear flows, J. Fluid Mech. **212**, 533 (1990).
[27] R. M. Gailis, A. Hill, E. Yee, and T. Hilderman, Extension of a fluctuating plume model of tracer dispersion to a sheared boundary layer and to a large array of obstacles, Bound.-Lay. Meterol. **122**, 577 (2007).
[28] S. Pope, Lagrangian PDF methods for turbulent flows, Annu. Rev. Fluid Mech. **26**, 23 (1994).
[29] W. Kollmann, The PDF approach to turbulent flow, Theor. Comput. Fluid Dyn. **1**, 249 (1990).
[30] S. Pope, *Turbulent Flows* (Cambridge University Press, Cambridge, 2000).
[31] R. O. Fox and A. Varma, *Computational Models for Turbulent Reacting Flows* (Cambridge University Press, Cambridge, 2003).
[32] D. Haworth, Progress in probability density function methods for turbulent reacting flows, Prog. Energy Combust. **36**, 168 (2010).
[33] D. Roekaerts, Use of a Monte Carlo PDF method in a study of the influence of turbulent fluctuations on selectivity in a jet-stirred reactor, Appl. Sci. Res. **48**, 271 (1991).
[34] K. Tsai and R. Fox, PDF modeling of turbulent-mixing effects on initiator efficiency in a tubular LDPE reactor, AIChE J. **42**, 2926 (1996).
[35] P. Colucci, F. Jaberi, P. Givi, and S. Pope, Filtered density function for large eddy simulation of turbulent reacting flows, Phys. Fluids **10**, 499 (1998).
[36] G. I. Taylor, Diffusion by continuous movements, P. Lond. Math. Soc. **2**, 196 (1922).

[37] M. Abramowitz and I. Stegun, *Handbook of Mathematical Functions: With Formulas, Graphs, and Mathematical Tables*, Vol. 55 (Courier Corporation, Chelmsford, MA, 1965).
[38] C. Nironi, P. Salizzoni, M. Marro, P. Mejean, N. Grosjean, and L. Soulhac, Dispersion of a passive scalar fluctuating plume in a turbulent boundary layer. Part I: Velocity and concentration measurements, Bound.-Lay. Meterol. **156**, 415 (2015).
[39] J. Jimènez, Turbulent flows over rough wall, Annu. Rev. Fluid Mech. **36**, 173 (2004).
[40] J. Fackrell, A flame ionisation detector for measuring fluctuating concentration, J. Phys. E: Sci. Instrum. **13**, 888 (1980).
[41] G. Iacobello, M. Marro, L. Ridolfi, P. Salizzoni, and S. Scarsoglio, Experimental investigation of vertical turbulent transport of a passive scalar in a boundary layer: Statistics and visibility graph analysis, Phys. Rev. Fluids **4**, 104501 (2019).
[42] J. Fackrell and A. G. Robins, Concentration fluctuations and fluxes in plumes from point sources in a turbulent boundary layer, J. Fluid Mech. **117**, 1 (1982).
[43] J. Fackrell and A. Robins, The effects of source size on concentration fluctuations in plumes, Bound.-Lay. Meterol. **22**, 335 (1982).
[44] F. Gifford, Statistical properties of a fluctuating plume dispersion model, *Advances in Geophysics*, Vol. 6 (Elsevier, Amsterdam, 1959), pp. 117–137.
[45] M. Cassiani, P. Franzese, and U. Giostra, A PDF micromixing model of dispersion for atmospheric flow. Part I: Development of the model, application to homogeneous turbulence and to neutral boundary layer, Atmos. Environ. **39**, 1457 (2005).
[46] S. Pope, Mapping closures for turbulent mixing and reaction, Theor. Comput. Fluid Dyn. **2**, 255 (1991).
[47] F. Jaberi and P. Givi, Inter-layer diffusion model of scalar mixing in homogeneous turbulence, Combust. Sci. Technol. **104**, 249 (1995).
[48] S. Du, D. J. Wilson, and E. Yee, A stochastic time series model for threshold crossing statistics of concentration fluctuations in non-intermittent plumes, Bound.-Lay. Meterol. **92**, 229 (1999).
[49] M. Cassiani, P. Franzese, and J. Albertson, A coupled Eulerian and Lagrangian mixing model for intermittent concentration time series, Phys. Fluids **21**, 085105 (2009).